PCCP

Accepted Manuscript

ROYAL SOCIETY OF CHEMISTRY

www.rsc.org/pccp

Influence of Size and Charge of Gold Nanocluster on Complexation with siRNA: A Molecular Dynamics Simulation Study

Sathish Kumar Mudedla [a, b], Ettayapuram Ramaprasad Azhagiya Singam[a], Kanagasabai Balamurugan[a] and Venkatesan Subramanian[a, b, *]

[a] *Chemical Laboratory, CSIR-Central Leather Research Institute, Adyar, Chennai-600 020, India*

[b] *Academy of Scientific and Innovative Research (AcSIR), CSIR-CLRI Campus, Chennai 600 020, India*

Abstract

The complexation of small interfering RNA (siRNA) with positively charged gold nanoclusters has been studied in the present investigation with the help of classical molecular dynamics and steered molecular dynamics simulations accompanied by the free energy calculations. Results show that the gold nanoclusters form a stable complex with siRNA. The wrapping of siRNA around gold nanocluster depends on the size and charge on the surface of gold cluster. The binding pattern of gold nanocluster with siRNA is also influenced by the presence of another cluster. The interaction between positively charged amines in the gold nanocluster and negatively charged phosphate group in the siRNA is responsible for the formation of complexes. The binding free energy value increases with size of the gold cluster and number of positive charges present on the surface of gold nanocluster. Results reveal that the binding energy of small gold nanoclusters increases in the presence of another gold nanocluster. While, the binding of large gold nanoclusters decreases due to the introduction of another gold nanocluster. Overall, findings have clearly demonstrated the effect of size and charge of gold nanoclusters on their interaction pattern with siRNA.

* To whom correspondence should be addressed. Tel.: +91 44 24411630. Fax: +91 44 24911589. E–mail: subuchem@hotmail.com, subbu@clri.res.in.

1 Introduction

The discovery of RNA interference by Fire and Mello has kindled numerous activities in biological sciences. It is a regulatory mechanism to control pathogenic and over expression genes activity.[1-3] RNA interference is a highly useful technique in curing many diseases such as cancers, genetic disorders, infections and autoimmune diseases.[4-8] Small interfering RNA (siRNA) has attracted a lot of interest as it mediates RNA interference.[9] The affected gene expressions can be silenced by the delivery of siRNA to the disease cells.[10,11] One of the major challenges is the delivery of siRNA to the desired location. The crossing of cell membrane is a significant challenge for siRNA due to its large size and negative charge. The siRNA molecules can also be destroyed by the nucleases and they are unstable in blood and extracellular environments. Therefore, an effective delivery system is necessary to carry the siRNA into the interior of the cells.

Polymers, lipids, peptides, proteins and nanomaterials have been used as siRNA delivery systems.[12-28] Polymers, such as polyethyleneimine and dendrimers have been employed as an attractive vehicle for the delivery of siRNA.[29-31] Molecular dynamics simulations have been performed to understand the complexation of siRNA and dendrimers.[32] Nanomaterials such as gold nanoparticles, silica nanoparticles, carbon nanotubes, magnetic nanoparticles and semiconductor quantum dots are used in the delivery of siRNA to the targeting cells.[33-37] The unzipping of siRNA has been observed in the molecular dynamics study on the carbon nanotube and siRNA complex due to π-π stacking interaction.[38] Since several reports have been published using gold nanoparticles as siRNA carrying agents due to their tunable reductive preparation, high chemical stability, biocompatibility and surface chemistry which allow for easy functionalization with biomolecules.[39] The optical properties of gold nanoparticles provide

applications in the field of bio-imaging.[40] Two strategies were developed to form the complexes of siRNA with gold nanoparticles: (i) siRNA conjugation to gold nanoparticle surface via gold–thiol covalent bond and to the conjugated molecules through sulphur-sulphur bonds and (ii) siRNA conjugation to the gold nanoparticle surface with electrostatic interaction.[41] Several experimental reports have revealed that the successful delivery of siRNA and DNA to the cells using electrostatic interaction as a mechanism.[41-46] In this connection, the applications of gold nanoclusters have been considered as a possible counterpart to develop appropriate delivery systems. Further, The positively charged gold nanoparticle effectively passes through an extra-cellular lipid membrane than the negative and neutral charged particles.[47] The penetration of gold nanoparticles into the cells depends on size, shape and charge present on its surface.[48-50] It is also possible that gold nanoparticle functionalized with the positively charged ligands can effectively interact with negatively charged siRNA with the help of above-mentioned electrostatic approach.

Recently, gold nanoclusters (size below 2 nm) which contain a few numbers of atoms have been synthesized and they acts as a bridge between atomic and nanoparticle behaviors.[51-55] Gold nanoparticles have the property of palsmonic resonance whereas the gold nanoclusters exhibit photoluminescence.[56] Gold nanoclusters have received wide spread attention because of their importance in various applications such as bio-sensing, and bio-imaging.[57,58] Recently, we have investigated the interaction between gold nanocluster and protein as well as associated changes in the structure and dynamics of protein.[59] Previous study has revealed that the smaller gold nanoparticles (50 nm) have advantages over the larger nanoparticles (100 nm) in the uptake and permeability in tumor tissues.[60] Therefore, the gold nanoclusters can penetrate into lipid membranes easily when compared to gold nanoparticles due to their small size. The passage of herceptin into the nucleus using herceptin-conjugated gold nanoclusters enhances the anticancer

activity of drug.[61] Tao et. al have reported that the synthesis of polyethyleneimine conjugated gold nanoclusters (size below 2 nm) which can be used for the efficient delivery of genes.[62] The gold nanocluster minimizes the cytotoxicity of polyethyleneimine and enhances the gene transfection efficiency. The excellent photo luminescent properties of gold nanoclusters provide a versatile strategy for fluorescent imaging and the fluorescent probe tracks the transfection behavior. The binding pattern of siRNA and energetics for the formation of non-covalent complexes of siRNA with gold nanocluster remain still elusive. The understanding of the complexation process of siRNA and gold nanoclusters would be useful to develop new carriers for gene delivery. Therefore, in this study, the complexation process of siRNA with positively charged gold nanoclusters has been investigated using classical molecular dynamics and steered molecular dynamics simulations. The following points have been addressed in this study:

1) Understanding the complexation of siRNA with positively charged gold nanoclusters.
2) Exploring the structural changes in the siRNA upon interaction with positively charged gold nanoclusters.
3) Predicting the energetics of the complex formed between siRNA and positively charged gold nanocluster.

2 Computational Details

The coordinates for the structure of siRNA were taken from protein data bank (pdb id: 2F8S).[63] In order to understand the interaction between siRNA and gold nanoclusters, the complexes of Au_{38} $(SC_5NH_{13})_{24}$ and Au_{102} $(SC_5NH_{13})_{44}$ with siRNA were considered in this study. Thiolated Au_{38} and Au_{102} clusters were known to form stable structures, hence, the same clusters were selected.[64,65] To investigate the interaction of siRNA with gold nanocluster in the

environment of another cluster, the complexes of $(Au_{38}(SC_5NH_{13})_{24})_2$ and $(Au_{102}(SC_5NH13)_{44})_2$ with siRNA were considered. The optimized geometries of gold nanoclusters $(Au_{38}(SC_5NH_{13})_{24}$, $Au_{102}(SC_5NH_{13})_{44})$ were taken from the previous investigation.[66] The gold nanoclusters $Au_{38}(SC_5NH_{13})_{24}$, $Au_{102}(SC_5NH_{13})_{44}$, $(Au_{38}(SC_5NH_{13})_{24})_2$ and $(Au_{102}(SC_5NH_{13})_{44})_2$ are represented as AU38, AU102, 2AU38 and 2AU102 in the remaining part of the text. Molecular dynamics simulations were performed using GROMACS-4.6.2 package.[67-69] All atom AMBER03 force field was used for the siRNA.[70] The force field parameters for ammonium alkyl thiolate group (SC_5NH_{13}) were derived using antechamber.[71,72] The partial charges for the alkyl group were derived using restrained electrostatic potential method at B3LYP/6-31G* level of theory with Gaussian 09 suit of programs.[73-79] The force constants for the bonds (Au-Au and Au-S) and angle (Au-S-Au) were taken from the literature and used to maintain the rigid structure of gold nanoclusters.[80,81] The Lenard Jones parameters for gold atoms were taken from the previous studies and they were treated as charge less particles.[82,83] The structures of both siRNA and gold nanoclusters were placed in a cubic box and solvated using a TIP3P water model. The overall positive or negative charge of the complexes was neutralized using the ions Na^+ and Cl^-. All the complexes were subjected to the energy minimization using steepest decent method to relax the whole system. The minimized structures were equilibrated by imposing the position restrains for 1 ns at 293 K temperature and 1 bar pressure. Velocity Rescale (V-rescale) and Parrinello-Rahman algorithms were used to control the temperature and pressure with a coupling constant of 0.1 and 2.0 pico second, respectively.[84-86] Production run was carried out for 60 nano second (ns) with a time step of 2 femto second (fs) in NPT ensemble. Particle Mesh Ewald method was used to calculate the electrostatic interactions with interpolation order of 4 and a grid spacing of 1.6 Å.[87] Bonds between hydrogen and heavy atoms were constrained at equilibrium bond lengths

using the LINCS algorithm.[88] The obtained trajectories were visualized by using VMD package.[89]

The configurations obtained from MD simulations were taken for the steered molecular dynamics (SMD) simulations. The same force field parameters were used for the siRNA and gold nanoclusters. The complexes of siRNA and gold nanoclusters were solvated with water using TIP3P model. After the energy minimization, the complexes were equilibrated for 1 ns in NPT ensemble by imposing position restrains. SMD simulations were carried out for 4 ns with a time step of 2 fs in NPT ensemble. During the SMD simulation, the position of siRNA was restrained and gold nanocluster was pulled with velocity of 0.005 nm/ps. The harmonic spring constant of 2500 kJ/mol was used to pull the siRNA from gold nanocluster. The snap shots of configurations in the trajectories obtain from SMD simulations were taken for the umbrella sampling windows.

3 Results and Discussion

Initially, the distance between the center of masses of gold nanocluster and siRNA was kept at a distance of 40 Å, to understand the complexation of siRNA with AU38, AU102, 2AU38 and 2AU102. The distance decreases during the dynamics due to the electrostatic interaction between the positively charged gold nanocluster and negatively charged siRNA. The process of complexation can be understood from the number of contacts between gold nanocluster and siRNA. The calculated number of contacts within 4 Å is shown in supporting information (Fig. S1). It can be noted that the number of contacts increases when compared to the starting geometries for all the gold nanoclusters. The calculated average number of contacts between gold nanoclusters and siRNA are 738, 762, 749 and 616 for AU38, AU102, 2AU38 and 2AU102, respectively. The number of contacts is higher for AU102 when compared to AU38,

2AU38 and 2AU102 complexes. Available surface area for the interaction of siRNA increases in accordance with the size of gold nanocluster. The number of positive charged particles in the gold nanoclusters available on the surface also increases with the increase in size of the cluster. Hence, the binding of siRNA with AU102 enhances when compared to that of AU38. The complexation of siRNA with gold nanocluster can be seen from the snap shots of the trajectory at different intervals of time. The snap shots from the trajectory of AU38 are depicted in Fig. 1 and it illustrates that the Au_{38} is encapsulated by the two terminals of siRNA. The snap shots from the trajectories of AU102, 2AU38 and 2AU102 are displayed in Fig. 1. The complete wrapping of siRNA does not take place, further it adsorbs onto the surface of gold nanocluster (AU102, 2AU38 and 2AU102). Among various clusters, Au_{38} facilitates the wrapping of siRNA around the gold nanocluster due to its smaller size. The length of siRNA is not enough to wrap the larger sized gold nanocluster (Au_{102}). In the case of 2AU38, two gold nanoclusters interact with both sides of siRNA. To reduce the repulsion between two positively charged Au_{38} clusters, in the starting of simulation those clusters were placed on the both sides of siRNA. The siRNA is unable to wrap any one of the Au_{38} cluster like in the case of AU38 because of the competition between two gold nanoclusters. The binding of 2AU102 nanocluster with siRNA is different from that of AU102. The siRNA lies between the two Au_{102} nanoclusters. The maximum number of contacts is observed in AU102 owing to its size in contrast to AU38. The minimum number of contacts is found in 2AU102. The two Au_{102} clusters interact from both sides of siRNA. As a consequence siRNA unable to wrap onto the surface of any one of the Au_{102} cluster. Therefore, the wrapping of siRNA depends on the size and number of gold nanoclusters present around in the vicinity of siRNA. The calculated radius of gyration for siRNA in all the models (AU38, AU102, 2AU38 and 2AU102) are presented in supporting information (Fig. S2). The radius of

gyration of siRNA decreases with the progression of time due to the binding with the surface of gold nanoclusters (AU38, AU102, 2AU38 and 2AU102) and it reaches a plateau value. The decrease in radius of gyration is more in the case of AU38 in contrast to other models due to the complete wrapping of siRNA around Au_{38} cluster.

The number of water molecules within 3 Å around the gold nanocluster as a function of time is presented in supporting information (Fig. S3). It can be seen that the number of water molecules decreases up to 5 ns to facilitate the interaction of nanoclusters with siRNA. The number of water molecules at 0 ns for AU38, AU102, 2AU38 and 2AU102 is 241, 363, 415 and 692, respectively. The average number of water molecules present around the gold nanocluster throughout the simulations is 162, 287, 354 and 593 for AU38, AU102, 2AU38 and 2AU102, respectively. The average number of water molecules decreases with reference to initial values. The reduction in number of water molecules is high for 2AU102 because siRNA interacts with two clusters. The decrease in the number of water molecules is more in the case of AU38 compared to AU102 and 2AU38. It is due to complete wrapping of siRNA around the Au_{38} cluster. The decrease in number of water molecules in the hydration shell around gold nanocluster assists the binding with siRNA which is in close agreement with contact analysis.

Previous report has been showed that the NH_3 group present in gold nanocluster can coordinate to three water molecules through hydrogen bond formation.[81] In order to understand the coordination of water molecules with NH_3 group, the number of hydrogen bonds between gold nanocluster and water molecules were calculated. The calculated number of hydrogen bonds depicted in Fig 2. It can be observed that the number of hydrogen bonds decreases with respect to initial values. The initial number of hydrogen bonds (at 0 ns) is 71, 123, 134 and 249 in AU38, AU102, 2AU38 and 2AU102, respectively. The average of hydrogen bonds is 54, 101,

118 and 204 for AU38, AU102, 2AU38 and 2AU102, respectively. The decrease in the hydrogen bonds is high in the case of 2AU102. The reduction in hydrogen bonds shows that the coordination shell structure of water around gold nanocluster disturbed due to the binding of siRNA.

To unravel the complexation process, the gold nanoclusters were considered at different initial positions with respect to siRNA. The different initial structures for AU38, 2AU38 are given in supporting information (Fig. S4). All the models were simulated for 60 ns. The complete wrapping of siRNA can be found from supporting information (Fig. S4) in the case AU38. For 2AU38, two gold nanoclusters were interacted with the siRNA on both sides. After simulation, it is evident that the two gold nanoclusters interact with siRNA on the both sides without any wrapping in stark contrast to the interaction of single gold cluster with siRNA due to the repulsion between two clusters.

In order to understand the influence of presence of another gold nanocluster on the binding process, Au_{38} (Au_{102}) cluster was interacted with the final snap shot of siRNA-AU38 (siRNA-AU102) complex. In this context, two models were considered. These models are represented as AU38+Au_{38} and AU102+Au_{102}. The snap shots of the trajectory at 0 ns and 60 ns are shown in Fig. 3. It can be noticed that the presence of another gold nanocluster does not disrupt structure of siRNA-gold nanocluster complex. The introduction of new cluster binds at the other side of siRNA. The calculated number of contacts between siRNA and two gold nanoclusters are given in supporting information (Fig S5). Significant changes are not observed in the number of contacts of cluster-1(from siRNA-AU38 (siRNA-AU102) complex) with siRNA after the interaction of cluster-2 (new cluster (Au_{38} or Au_{102})). Furthermore, the number

of contacts increases in the case of cluster-2. These results point out that the presence of another gold nanocluster does not disrupt or enhance the binding of cluster with siRNA.

To understand the predominant interactions involved in the formation of complexes of siRNA with gold nanocluster, van der Waals and electrostatic energy between siRNA and gold nanocluster were calculated from MD simulations. The calculated van der Waals and electrostatic energies are plotted in Fig. 4 and supporting information (Fig S6). The Lennard jones and columbic interaction potentials were used to calculate the van der Waals and electrostatic energies between siRNA and gold nanocluster, respectively. It can be seen from Fig. S6 that both electrostatic and van der Waals energies increase due to interaction of siRNA with gold nanoclusters. In the case of 2AU102, marginal decrease in van der Waals energy is observed. The increase in both van der Waals and electrostatic energies favor the formation of complex between siRNA and gold nanocluster. Particularly, the contribution of electrostatic energy is dominant when compared to van der Waals energy for the complex formation. Thus the origin for the binding of siRNA with gold nanoclusters is electrostatic interaction in nature.

The radial distribution function (RDF) gives the information about how the density of molecules varies with respect to distance. The electrostatic interaction between positively charged gold nanocluster and negatively charged siRNA is responsible for the formation of complex. To understand the microscopic picture in binding of gold nanocluster with siRNA, radial distribution functions were calculated between the positively charged amines (gold nanocluster) and negatively charged phosphate group (siRNA). The calculated radial distribution function is displayed in Fig. 5. It illustrates that the RDF value of phosphate group is high within the 0.5 nm distance in all the cases which is in good agreement with the energetics for the complex of siRNA with gold nanocluster.

To investigate the effect of charge on the interaction between the two systems, the number of positive charges (24) on the surface of Au_{38} cluster was reduced to 8 by replacing the NH_3 groups with CH_3. The molecular formula of cluster is $Au_{38}(SC_6H_{13})_{16}(SC_5NH_{13})_8$ and it is represented as AU38-8NH3 in the remaining part of text. Interestingly, the complete wrapping of siRNA around the Au_{38} cluster is not observed in the case of AU38-8NH3. The snap shots for the siRNA-AU38-8NH3 complex is depicted in Fig. 6. Therefore, the wrapping of siRNA depends on the size and number of positive charges present on the gold nanocluster.

It is well known that the stability of helical structure of the siRNA depends on the stacking and hydrogen bond interactions between nucleobases. To understand the structural stability of siRNA, the number of hydrogen bonds and stacking energy were calculated as a function of time. The number of hydrogen bonds between two strands of siRNA is shown in supporting information (Fig. S7). Significant changes are not observed in the number of hydrogen bonds throughout simulation in all cases (AU38, AU102, 2AU38 and 2AU102). At the time t = 0 of simulations, the number of hydrogen bonds is found to be 47 and it is agreement with the previous study.[37] The average number of hydrogen bonds is found to be 37, 41, 42 and 45 in the cases of complexes formed by AU38, AU102, 2AU38 and 2AU102 with siRNA. The least number of bonds is found in AU38 complex due to the complete wrapping of siRNA. The stacking interaction in the strand of siRNA is defined as its total van der Waals energy.[90] The calculated van der Waals energy is shown in supporting information (Fig. S8). The calculated stacking energies for siRNA, 2AU38 and 2AU102 are in the range from -250.0 to -550.0 kJ. mol^{-1}. Therefore, there are no significant changes in strands of siRNA after the interaction with gold nanocluster in the case of 2AU38 and 2AU102. It can be noticed that the stacking energy ranges from -220.0 to -550.0 kJ. mol^{-1} (strand-1) and -160.0 to -530.0 kJ. mol^{-1} (strand-2) in the case of

AU38 whereas the same fluctuates around -200.0 to -500.0 kJ. mol^{-1} (strand-1) and -150.0 to -500.0 kJ. mol^{-1} (strand-2) for AU102. The stacking energy decreases marginally in the case of AU38 and AU102. The reduction in energy points out that there are marginal perturbations in the stacking pattern of nucleobases present in siRNA.

In order to understand the structural changes in minor and major grooves of siRNA, their widths were calculated (Fig. S9). The widths of minor and major groove were estimated by measuring the direct phosphorous (P)—phosphorous (P) distance between sugar groups in two strands of siRNA. The average values of major and minor groove widths for all the cases are listed in Table S1 along with the initial values. It can be seen that there is a marginal increase in the major groove and a decrease in minor groove for AU102, 2AU38 and 2AU102. In the case of AU38, both major and minor groove values decrease when compared to starting values. Marginal changes are observed in the major and minor grooves in the case of AU38 with respect to to starting values. Overall, significant changes have not observed in the minor and major groove of siRNA after interaction with gold nanoclusters. The distribution of back bone dihedral angles include alpha (α), beta (β), gamma (γ), delta (δ), epsilon (ε) and zeta (ζ) of both strands of siRNA were calculated (Fig. S10). It can be seen from Fig. S9 that the dihedral angles of siRNA significantly vary upon interaction with gold nanoclusters. The variations in the dihedral angles are due to the wrapping of siRNA around gold nanocluster.

The conformational entropy was calculated using quasi harmonic oscillator approximation method.[91] In this method, the associated vibrational frequency is estimated by the principle component analysis (PCA). The PCA was performed on the trajectories obtained from MD simulations for all the models (siRNA, AU38, AU102, 2AU38 and 2AU102). The calculated conformational entropy values are 9.06, 10.11, 8.42, 8.37 and 7.71 kJ. mol^{-1} K for

siRNA, AU38, AU102, 2AU38 and 2AU102, respectively. It can be seen that the conformational entropy of siRNA decrease upon binding with gold nanocluster except for AU38 model. The lower value of conformational entropy indicates the rigidity of the siRNA upon interaction with gold nanocluster. The motions of the siRNA have been restrained through the interaction with gold nanocluster. The calculated residue wise root mean square fluctuations (RMSFs) of siRNA for all the models siRNA, AU38, AU102, 2AU38 and 2AU102 are depicted in Fig. S11. It can be seen that the fluctuations of siRNA have been reduced upon interaction with the gold nanocluster and these fluctuations are in close corroboration with conformational entropy values.

Cluster analysis was carried out on the trajectory for all the complexes obtained from MD simulations. The predominant structures were collected from cluster analysis and used as initial structures for SMD simulations. SMD simulations were performed for the complexes of siRNA and gold nanoclusters. In these simulations, the center of mass (COM) of gold nanocluster was pulled in the direction perpendicular to COM of siRNA. During the pulling of gold nanocluster, the position of siRNA was restrained. In the case of two gold nanocluster models (2AU38 and 2AU102), one cluster was pulled away from complex and subsequently other bound cluster was pulled away from siRNA. The pulling simulations corresponding to 2AU38 and 2AU102 are denoted as 2AU38-1, 2AU38-2, 2AU102-1 and 2AU102-2, respectively. The pulling of gold nanocluster was performed using the velocity 0.005 nm/ps. The dissociation of gold nanocluster with the velocity 0.005 nm/ps form the siRNA in all the models is shown in Fig. S12, using the snap shots at different time intervals. The force profiles for the complexes of siRNA and gold nanocluster are presented in Fig. 7. The maximum force is higher for the gold nanocluster in the complex of AU102 when compared to other models. The order of maximum force required to pull the siRNA is found to be AU102 > 2AU38-2 > AU38 > 2AU102-2 > 2AU38-1 > 2AU102-

1. The configurations obtained from the SMD simulations were used for umbrella sampling. From the SMD trajectories, 62, 56, 67, 49, 63 and 49 configurations were collected using space of 0.2 nm between the COM of siRNA and gold nanocluster for the complexes AU38, AU102, 2AU38-1, 2AU38-2, 2AU102-1 and 2AU102-2. Umbrella sampling simulations were carried out for 3 ns on each window collected form SMD simulations. The data obtained from simulation of each window was analyzed using weighted histogram analysis method (WHAM) of Kumar et al.[92] The calculated free energy of dissociation for gold nanocluster from siRNA using the WHAM method is presented in Fig. 8. The calculated binding energy values are -149.55, -270.7, -66.56 -120.6, -65.3 and -189.9 kcal. mol^{-1} for the AU38, AU102, 2AU38-1, 2AU38-2, 2AU102-1 and 2AU102-2 complexes, respectively. The total binding free energy (sum of binding energies of 2AU38-1(2AU102-1) and 2AU38-2(2AU102-2)) for 2AU38 and 2AU102 is -187.16 and 255.2 kcal. mol^{-1}. The order of binding free energies is observed to be AU102 > 2AU102 > 2AU38 > AU38. It can be noted that the binding free energy for AU102 is high. The number of positive charges on Au_{38} is not sufficient for the effective binding with siRNA. But siRNA can bind strongly when the number of Au_{38} clusters is increased. Therefore, small sized gold nanoclusters can interact strongly when their number is more in the vicinity of siRNA. The binding strength of siRNA with AU102 is high when compared to AU38 due to more number of positive charges and large size of AU102. The presence of second AU102 influences the binding of other gold nanocluster in 2AU102. Hence, the binding of siRNA can be enhanced by increasing the size and number of positive charges of gold nanoclusters. The large size gold nanoclusters can effectively bind if the number nanoclusters are less around siRNA.

4 Conclusion

The complexation process of positively charged gold nanocluster with siRNA has been studied using molecular dynamics, steered molecular dynamics and umbrella sampling simulations. It is found that the wrapping of siRNA depends on size of the gold nanocluster and its charge. The binding mode of gold nanocluster with siRNA depends on the number of gold nanoclusters present in the interaction environment. The electrostatic interaction between positively charged amines in gold nanocluster and negatively charged phosphate groups of siRNA is responsible for the formation of complex. The stacking pattern of nucleobases and back bone dihedral angles of siRNA are disturbed marginally upon interaction with gold nanocluster. The conformational entropy of siRNA decreases upon interaction with gold nanocluster. The residue wise fluctuations of siRNA are reduced through the binding with gold nanoclusters. The binding free energy calculations have shown that the binding energy increases with size of gold nanocluster and the number of positive charges present on its surface. The effective binding process can be observed for the small size gold nanoclusters in the environment of another cluster. Whereas in the case of large sized clusters, the strength of the binding with siRNA decreases in the presence of another cluster. These results can be exploited for the applications of gene delivery.

Acknowledgment

We thank the Nanomaterial–Safety, Health and Environment (NanoSHE BSC0112) project funded by Council of Scientific and Industrial Research (CSIR) New Delhi, India, and Board of Research in Nuclear sciences (BRNS), Mumbai, India, and for Financial Support. S. K. M thanks Department of Science and Technology (DST), New Delhi, India for providing

INSPIRE Fellowship (Inspire Fellow). E. R. A. S and K. B thanks CSIR and NanoSHE for providing senior research fellowship.

Electronic supplementary information (ESI) available

Table S1 and Fig. S1-S12 are presented in the supporting information.

Supplementary Files

The movies of pulling and adsorption of gold nanocluster and siRNA complexes are presented in supplementary files.

References

1. G. Meister and T. Tuschl, *Nature,* 2004, **431**, 343.
2. G. J. Hannon and J. J. Rossi, *Nature,* 2004, **431**, 371.
3. A. Fire, S. Q. Xu, M. K. Montgomery, S. A. Kostas, S. E. Driver, and C. C. Mello, *Nature,* 1998, **391**, 806.
4. M. A. Behlke, *Mol. Ther.,* 2006, **13**, 644.
5. L. Aagaard and J. J. Rossi, *Adv. Drug Delivery Rev*., 2007, **59**, 75.
6. K. J. Von Eije, L. Aagaard, P. Saetrom, M. Amarzguioui, H. T. Li and J. J. Rossi, *Hum. Gene Ther.,* 2007, **18**, 1068.
7. A. de Fougerolles, H. P. Vornlocher, J. Maraganore and J. Lieberman, *Nat. Rev. Drug. Discov*., 2007, **6**, 443.
8. J. J. Rossi, *Biotechniques,* 2006, **40**, S25.
9. J. Martinez, A. Patkaniowska, H. Urlaub, R. Luhrmann and T. Tuschl, *Cell,* 2002, **110**, 563.
10. S. M. Elbashir, J. Harborth, W. Lendeckel, A. Yalcin, K. Weber and T. Tuschl, *Nature,* 2001, **411**, 494.
11. D. H. Kim and J. J. Rossi, *Nat. Rev. Genet.,* 2007, **8**, 173.
12. A. Tsubouchi, J. Sakakura, R. Yagi, Y. Mazaki, E. Schaefer, H. Yano and H. J. Sabe, *J. Cell. Biol*., 2002, **159**, 673.

13. M. S. Duxbury, H. Ito, E. Benoit, M. J. Zinner, S. W. Ashley and E. E. Whang, *Biochem. Biophys. Res. Commun*., 2003, **311**, 786.
14. A. C. R. Grayson, A. M. Doody and D. Putnam, *Pharm. Res.,* 2006, 23, 1868.
15. A. Santel, M. Aleku, O. Keil, J. Endruschat, V. Esche, B. Durieux, K. Loffler, M. Fechtner, T. Rohl, G. Fisch, S. Dames, W. Arnold, K. Giese, A. Klippel and J. Kaufmann, *Gene. Ther*., 2006, **13**, 1360.
16. N. F. Bouxsein, C. S. McAllister, K. K. Ewert, C. E. Samuel and C. R. Safinya, *Biochemistry*, 2007, **46**, 4785.
17. D. Palliser, D. Chowdhury, Q. Y. Wang, S. J. Lee, R. T. Bronson, D. M. Knipe and J. Lieberman, *Nature*, 2006, **439**, 89.
18. F. Simeoni, M. C. Morris, F. Heitz and G. Divita, *Nucleic Acids Res*., 2003, **31**, 2717.
19. A. Muratovska and M. R. Eccles, *FEBS Lett*., 2004, **558**, 63.
20. Y. L. Chiu, A. Ali, C. Y. Chu, H. Cao and T. M. Rana, *Chem. Biol.,* 2004, **11**, 1165.
21. Y. Minakuchi, F. Takeshita, N. Kosaka, H. Sasaki, Y. Yamamoto, M. Kouno, K. Honma, S. Nagahara, K. Hanai, A. Sano, T. Kato, M. Terada and T. Ochiya, *Nucleic Acids Res*., 2004, 32, e109/1.
22. I. Puebla, S. Esseghir, A. Mortlock, A. Brown, A. Crisanti and W. A . Low, *J. Biotechnol.,* 2003, **105**, 215.
23. Y. Takei, K. Kadomatsu, Y. Yuzawa, S. Matsuo and T. Muramatsu, *Cancer Res*., 2004, **64**, 3365.
24. Z. Liu, M. Winters, M. Holodniy and H. J. Dai, *Angew. Chem. Int. Ed.* 2007, **46**, 2023.
25. N. W. S. Kam, Z. Liu and H. Dai, *J. Am. Chem. Soc.,* 2005, **127**, 12492.
26. J. E. Podesta, K. T. A. Jamal, M. A. Herrero, B. W. Tian, H. Ali-Boucetta, V. Hegde, A. Bianco, M. Prato and K. Kostarelos, *Small* **2009**, *5*, 1176–1185.
27. H. M. Aliabadi, B. Landry, C. Sun, T. Tang and H. Uludag, *Biomaterials*, 2012, **33**, 2546e69.
28. J. H. Zhou, J. Y. Wu, N. Hafdi, J. P. Behr, P. Erbacher and L. Peng, *Chem. Commun.,* 2006, 2362.
29. A. Agrawal, D. H. Min, N. Singh, H. H. Zhu, A. Birjiniuk, G. von Maltzahn, T. J. Harris, D. Y. Xing, S. D. Woolfenden, P. A. Sharp, A. Charest and S. Bhatia, *ACS Nano*, 2009, ***3***, 2495.

30. V. Vasumathi and P. K. Maiti, *Macromolecules*, 2010, **43**, 8264.
31. M. Oishi, J. Nakaogami, T. Ishii and Y. Nagasaki, *Chem. Lett.*, 2006, **35**, 1046.
32. I. I. Slowing, B. G. Trewyn, S. Giri and V. S.-Y. Lin, *Adv. Funct. Mater*., 2007, **17**, 1225.
33. N. W. S. Kam, Z. Liu and H. Dai, *Angew. Chem. Int. Ed.*, 2006, **45**, 577.
34. K. Kostarelos, et al. *Nat. Nanotechnol*., 2007, **2***,* 108.
35. Z. Medarova, M. Kumar, S.-W. Ng, J. Yang, N. Barteneva, N. V. Evgenov, V. Petkova and A. Moore, *Transplantation*, 2008, **86**, 1170.
36. A. M. Derfus, A. A. Chen, D-H. Min, E. Ruoslahti and S. N. Bhatia, *Bioconjug. Chem*., 2007, **18**, 1391.
37. M. Santosh, S. Panigrahi, D. Bhattacharyya, A. K. Sood and P. K. Maiti, *J. Chem. Phys*., 2012, **136**, 065106.
38. D. Pissuwan, T. Niidome and M. B. Cortie, *J. Control. Release*., 2011, **149**, 65.
39. E. Hutter and D. Maysinger, *Microsc. Res. Tech.*, 2011, **74**, 592.
40. I. Ojea-Jiménez, O. Tort, J. Lorenzo and V. F. Puntes, *Biomed. Mater*., 2012, **7**, 054106.
41. A. Elbakry, A. Zaky, R. Liebl, R. Rachel, A. Goepferich and M. Breunig, *Nano Lett.*, 2009, **9**, 2059.
42. A. C. Bonoiu, S. D. Mahajan, H. Ding, I. Roy, K.-T. Yong, R. Kumar, R. Hu, E. J. Bergey, S. A. Schwartz and P. N. Prasad, *Proc. Natl Acad. Sci.*, 2009, **106**, 5546.
43. Y. Jiang, R. Tang, B. Duncan, Z. Jiang, B. Yan, R. Mout and V. M. Rotello, *Angew. Chem. Int. Ed. Engl.*, 2015, **54**, 506.
44. R. B. Shmueli, D. G. Anderson and J. J. Green, *Expert Opin Drug Deliv*., 2010, **7**, 535.
45. K. Niikura, K. Kobayashi, C. Takeuchi, N. Fujitani, S. Takahara, T. Ninomiya, K. Hagiwara, H. Mitomo, Y. Ito, Y. Osada and K. Ijiro, *ACS Appl. Mater. Interfaces*, 2014, **6**, 22146.
46. W. J. Song, J. Z. Du, T. M. Sun, P. Z. Zhang and J. Wang, *Small*, 2010, **6**, 239.
47. E. L. da Rocha, G. F. Caramori and C. R. Rambo, *Phys. Chem. Chem. Phys.*, 2013, **15**, 2282.
48. F. Zheng, J. Pan, X. Yin, J. Li, F. Wang and L. Zhao, *J. Nanosci. Nanotechnol.*, 2013, **13**, 3990.
49. S. Nangia and R. Sureshkumar, *Langmuir*, 2012, **28**, 17666.
50. J. Lin, H. Zhang, Z. Chen and Y. Zheng, *ACS Nano*, 2010, **4**, 5421.

51. J. Zheng, J. T. Petty and R. M. Dickson, *J. Am. Chem. Soc*., 2003, **125**, 7780.
52. Y. Negishi, Y. Takasugi, S. Sato, H. Yao, K. Kimura and T. Tsukuda, *J. Am. Chem. Soc.*, 2004, **126**, 6518.
53. P. L. Xavier, K. Chaudhari, A. Baksi and T. Pradeep, *Nano Rev*., 2012, **3**, 14767.
54. J. Zheng, C. W. Zhang and R. M. Dickson, *Phys. Rev. Lett.*, 2004, **93**, 077402.
55. J. Zheng, P. R. Nicovich and R. M. Dickson, *Annu. Rev. Phys. Chem*., 2007, **58**, 407.
56. Jin, R. *Nanoscale*, 2010, **2**, 343.
57. C. A. J. Lin, C. H. Lee, J. T. Hsieh, H. H. Wang, J. K. Li, J. L. Shen, W. H. Chan, H. I. Yeh and W. H. Chang, *J. Med. Biol. Eng.*, 2009, **29**, 276.
58. L. Shang, S. J. Dong and G. U. Nienhaus, *Nano Today*, 2011, **6**, 401.
59. S. K. Mudedla, E. R. Azhagiya Singam, J. Vijay Sundar, M. N. Pedersen, N. Arul Murugan, J. Kongsted, H. Ågren and V. Subramanian, *J. Phys. Chem. C*, 2015, **119**, 653.
60. S. Huo, H. Ma, K. Huang, J. Liu, T. Wei, S. Jin, J. Zhang, S. He and X. J. Liang, *Cancer Res*. 2013, **73**, 319.
61. Y. Wang, J. Chen and J. Irudayaraj, *ACS Nano*, 2011, **5**, 9718.
62. Y. Tao, Z. Li, E. Ju, J. Ren and X. Qu, *Nanoscale*, 2013, **5**, 6154.
63. Y. R. Yuan, Y. Pei, H. Y. Chen, T. Tuschl and D. J. Patel, *Structure*, 2006, **14**, 1557.
64. H. Qian, M. Zhu, U. N. Andersen and R. Jin, *J. Phys. Chem A*, 2009, **113**, 4281.
65. Y. Levi-Kalisman, P. D. Jadzinsky, N. Kalisman, H. Tsunoyama, T. Tsukuda, D. A. Bushnell and R. D. Kornberg, *J. Am. Chem. Soc.*, 2011, **133**, 2976.
66. J. Jung, S. Kang and Y. K. Han, *Nanoscale*, 2012**, 4**, 4206.
67. H. J. C. Berendsen, D. van der Spoel and R. van Drunen, *Comput. Phys. Commun.*, 1995, **91**, 43.
68. E. Lindahl, B. Hess and D. van der Spoel, *J. Mol. Model.*, 2001, **7**, 306.
69. B. Hess, C. Kutzner, D. van der Spoel and E. Lindahl, *J. Chem. Theory Comput.*, 2008, **4**, 435.
70. W. D. Cornell, P. Cieplak, C. I. Bayly, I. R. Gould, K. M. Merz, D. M. Ferguson, D. C. Spellmeyer, T. Fox, J. W. Caldwell and P. A. Kollman, *J. Am. Chem. Soc.*, 1995, **117**, 5179.
71. J. Wang, W. Wang, P. A. Kollman and D. A. Case, *J. Mol. Graphics Modell*. 2006, **25**, 247.

72. J. Wang, R. M. Wolf, J. W. Caldwell, P. A. Kollman and D. A. Case, *J. Comput. Chem.,* 2004, **25**, 1157.

73. A. D. Becke, *Phys. Rev. A*, 1988, **38**, 3098.

74. A. D. Becke, *J. Chem. Phys.*, 1993, **98**, 1372.

75. A. D. Becke. *J. Chem. Phys.*, 1993, **98**, 5648.

76. C. Lee, W. Yang and R.G. Paar, *Phys. Rev. B*, 1988, **37**, 785.

77. P. J. Hay and W. R. Wadt, *J. Chem. Phys*., 1985, **82**, 299.

78. T. H. Dunning and P. J. Hay, *In Modern Theoretical Chemistry*, H. F. Schaefer III, Ed.; Plenum: New York, 1976.

79. M. J. Frisch, G. W. Trucks, H. B. Schlegel, G. E. Scuseria, M. A. Robb, J. R. Cheeseman, G. Scalmani, V. Barone, B. Mennucci,; G. A. Petersson,; et al. Gaussian 09, revision A.02, Gaussian, Inc.: Wallingford CT, 2009.

80. J. G. Railsback, A. Singh, R. C. Pearce, T. E. McKnight, R. Collazo, Z. Sitar, Y. G. Yingling and A. V. Melechko, *Adv. Mater.*, 2012, **24**, 4261.

81. E. Heikkilä, A. A. Gurtovenko, H. Martinez-Seara, H. Häkkinen, I. Vattulainen and J. Akola, *J. Phys. Chem. C*, 2012, **116**, 9805.

82. O. S. Lee and G. C. Schatz, *J. Phys. Chem. C*, 2009, **113**, 15941.

83. P. K. Samanta, G. Periyasamy, A. K. Mannaa and S. K. Pati, *J. Mater. Chem.*, 2012, **22**, 6774.

84. S. Nose and M. L. Klein, *Mol. Phys.* 1983, **50**, 1055.

85. M. Parrinello and A. Rahman, *J. Appl. Phys.* 1981, **52**, 7182.

86. G. Bussi, D. Donadio and M. Parrinello, *J. Chem. Phys.*, 2007, **126**, 14101.

87. U. Essmann, L. Perera, M. L. Berkowitz, T. Darden, H. Lee and L. G. Pedersen, *J. Chem. Phys.*, 1995, **103**, 8577.

88. B. Hess, H. Bekker, H. J. C. Bendersen and J. G. E. M. Fraaije, *J. Comput. Chem.*, 1997, **18**, 1463.

89. W. Humphrey, A. Dalke and K. Schulten, *J. Mol. Graphics*, 1996, **14**, 33.

90. R. R. Johnson, A. T. Charlie Johnson and M. L. Klein, *Nano Lett.*, 2008, **8**, 69.

91. I. Andricioaei and M. Karplus, *J. Chem. Phys*., 2001, **115**, 6289.

92. S. Kumar, J. M. Rosenberg, D. Bouzida, R. H. Swendsen and P. A. Kollman, *J. Comput. Chem.*, 1992, **13**, 1011.

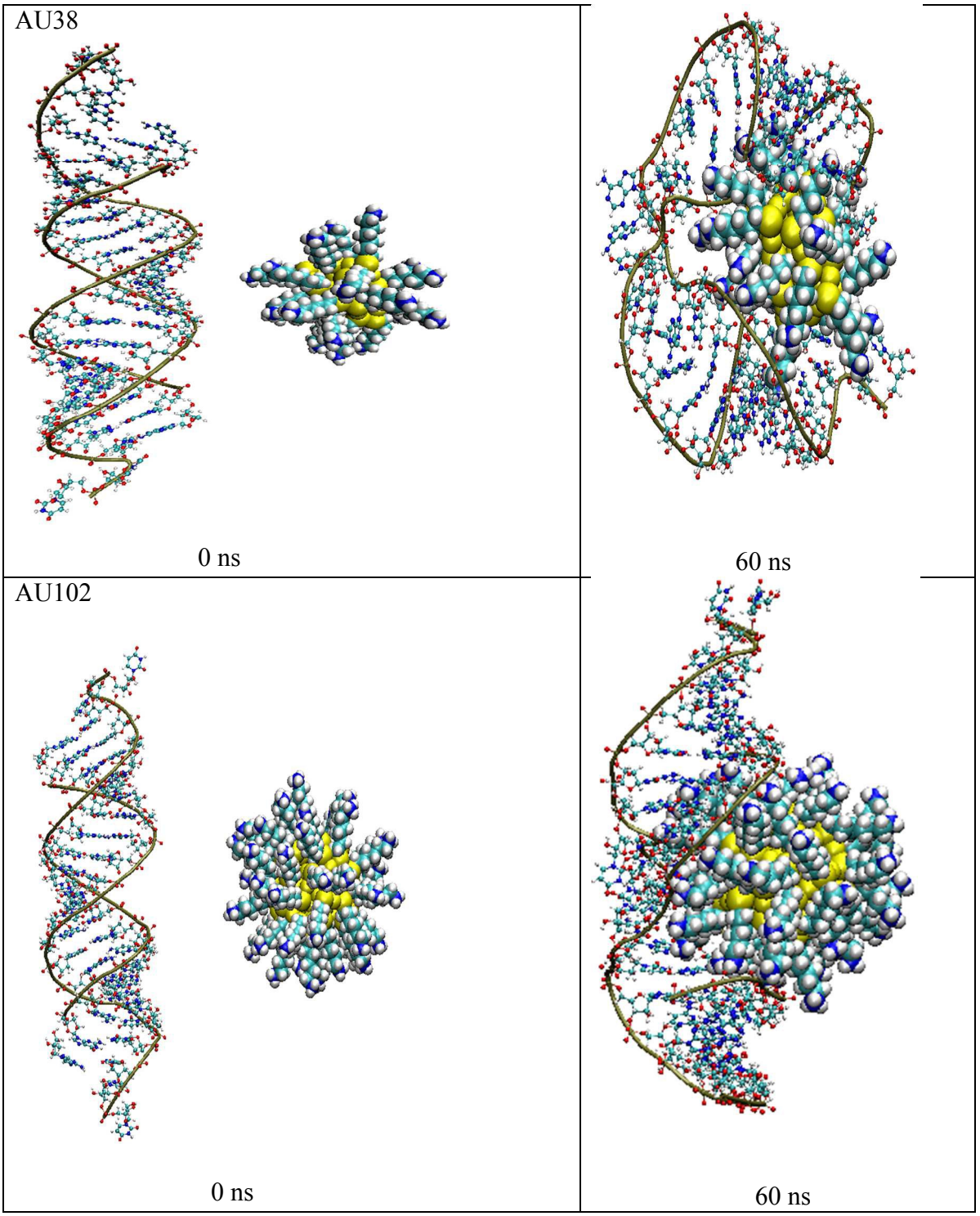

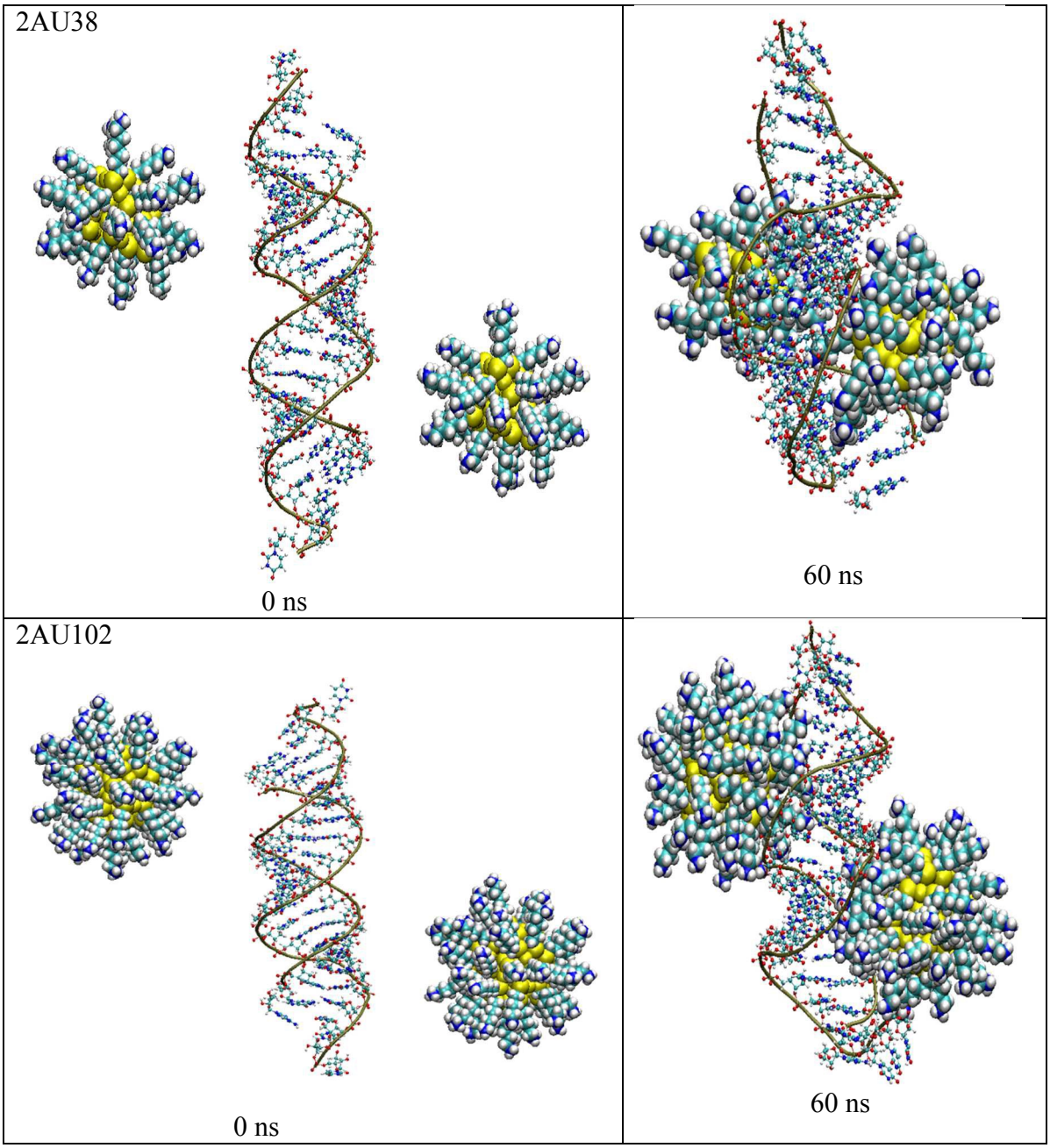

Fig. 1 The snapshots from the trajectory for the interaction of gold nanoclusters with siRNA.

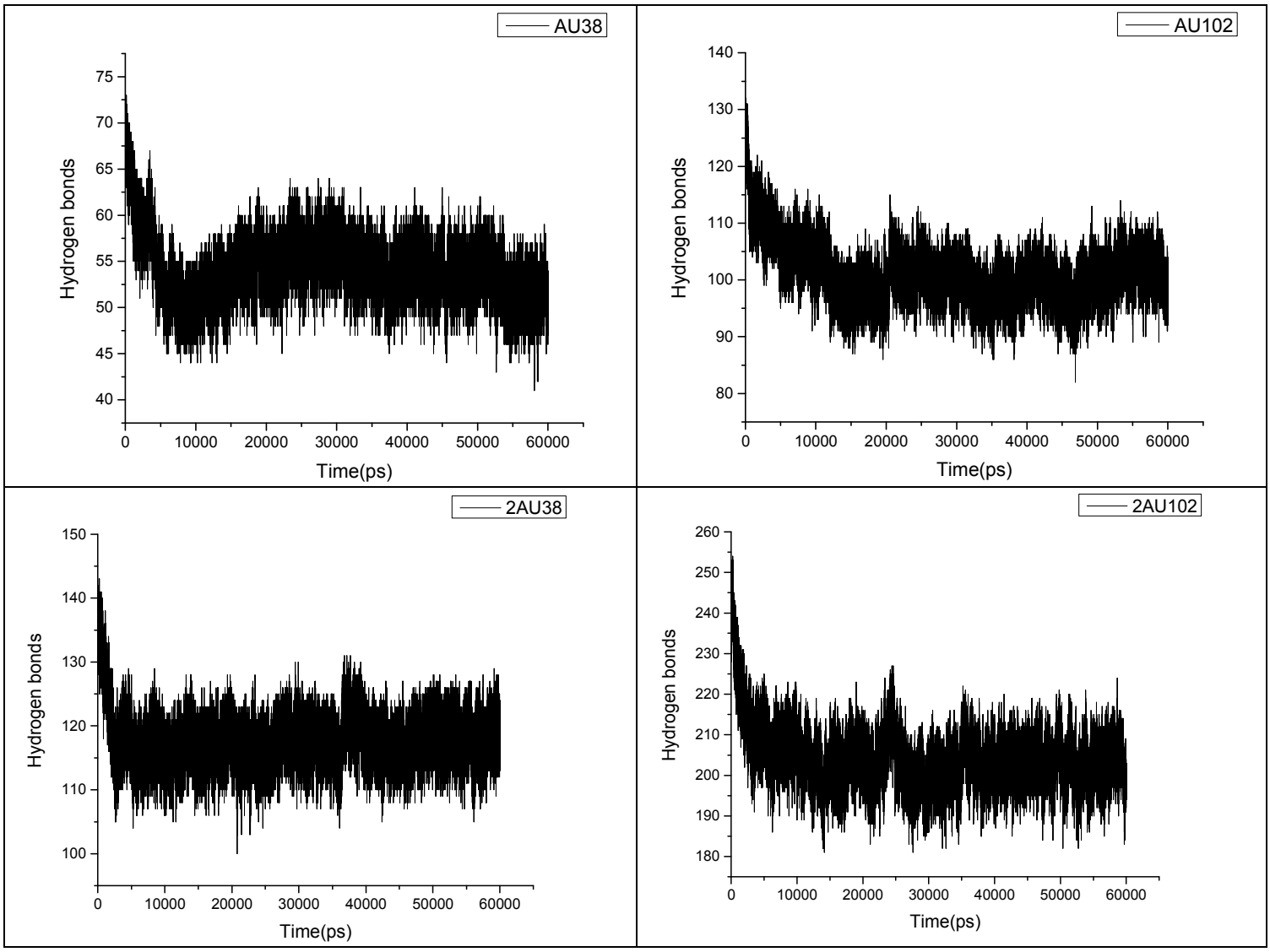

Fig. 2 The number of hydrogen bonds between gold nanocluster and water.

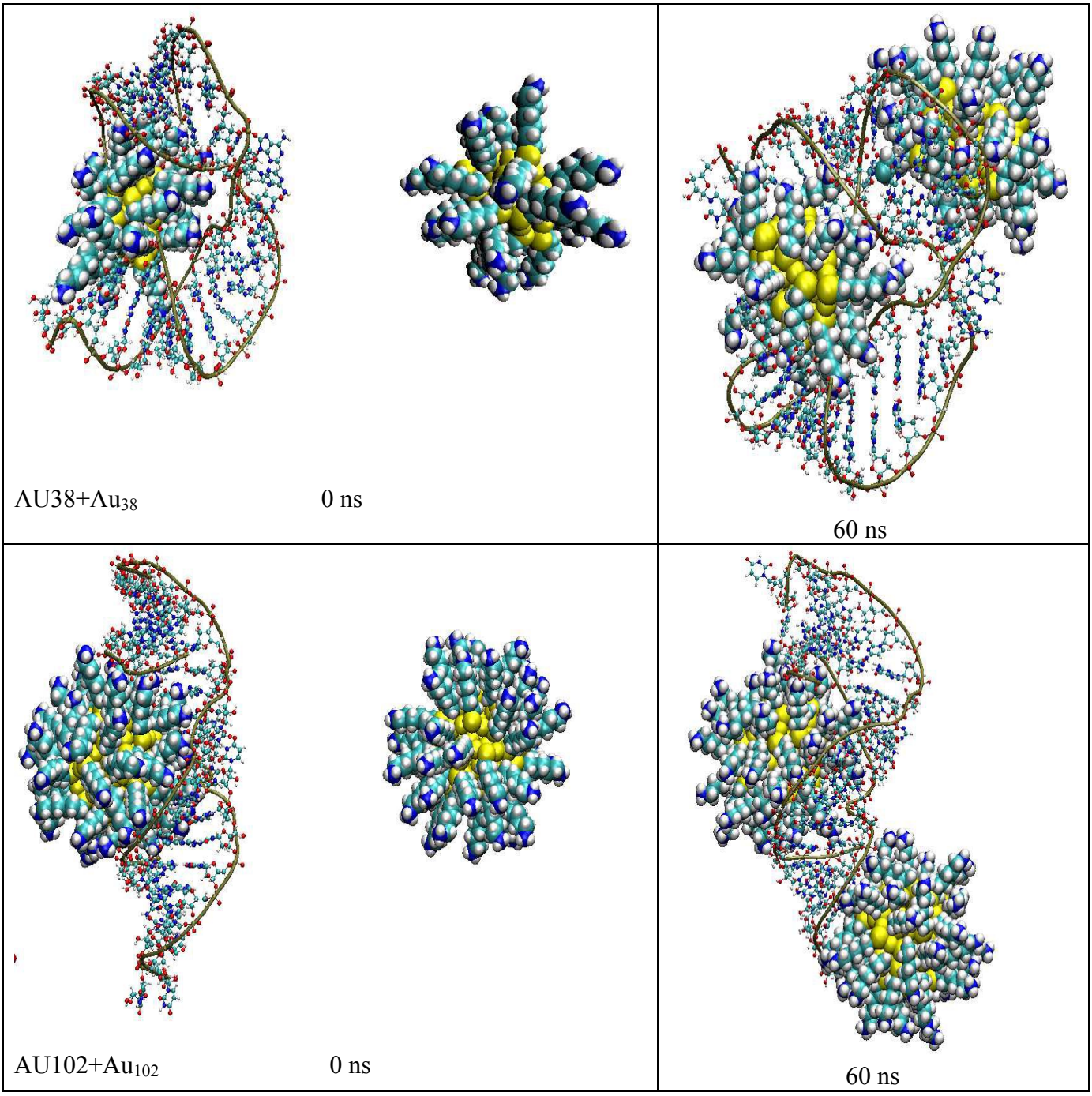

Fig. 3 The snapshots from the trajectory for the interaction of gold nanoclusters with siRNA in the presence of another cluster.

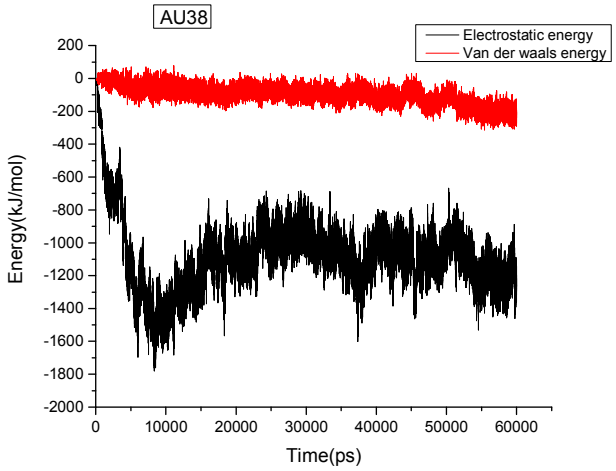

Fig. 4 The electrostatic and van der Waals interaction energy between positively charged gold nanoclusters and siRNA.

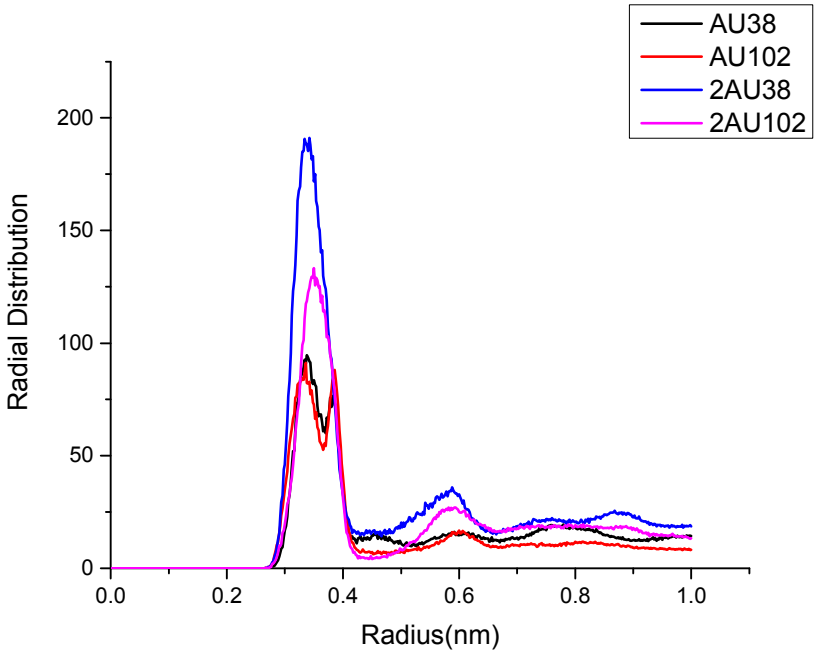

Fig. 5 The radial distribution of amine groups in gold nanocluster around the phosphate groups of siRNA.

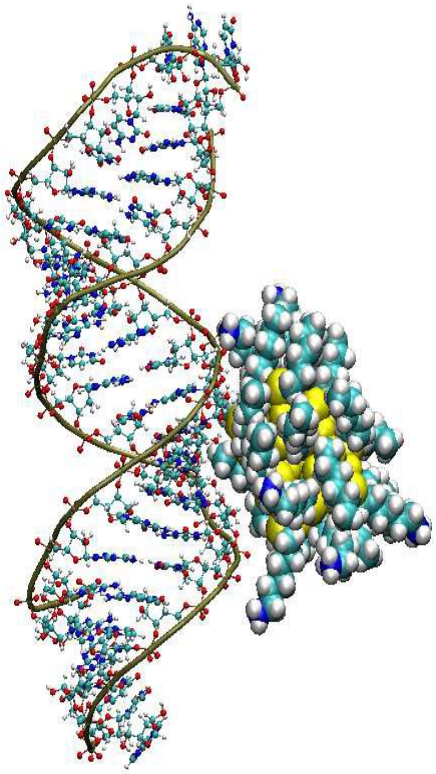

Fig. 6 The snapshot from the trajectory for the interaction of AU38-8NH3 with siRNA at 60 ns.

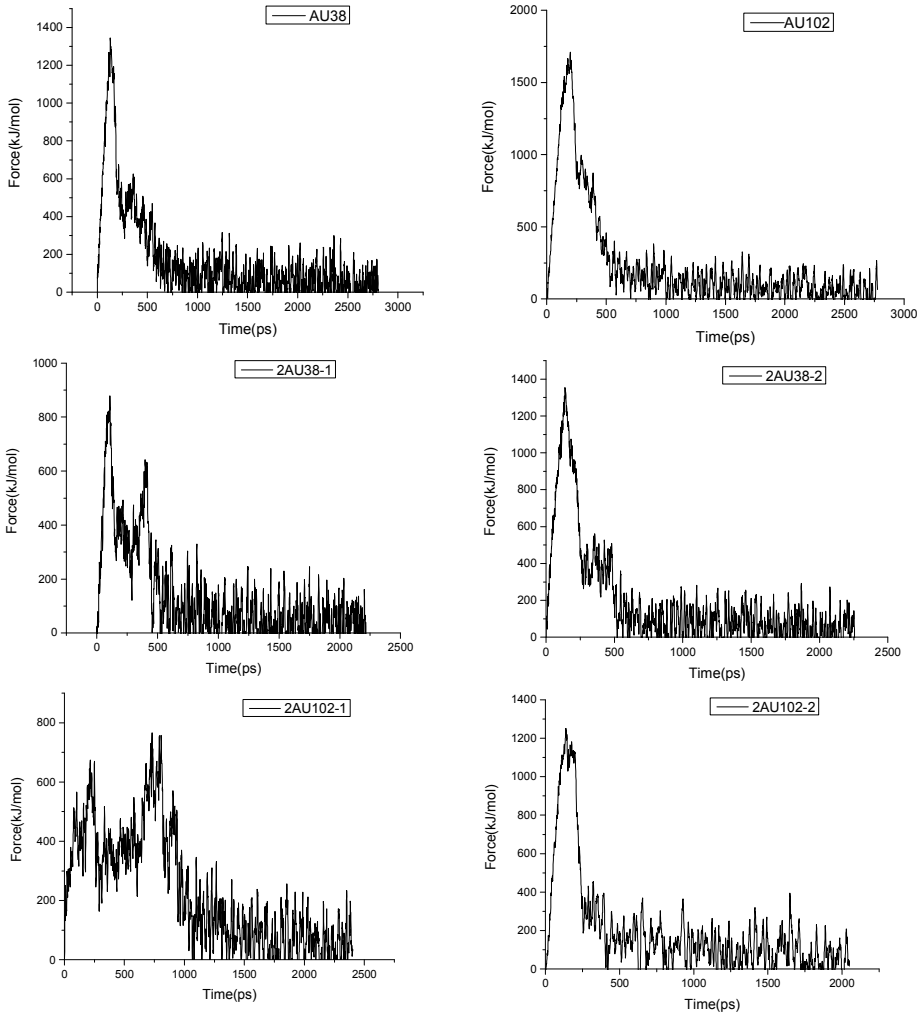

Fig. 7 Force profiles for all the complexes of siRNA-gold nanoclusters.

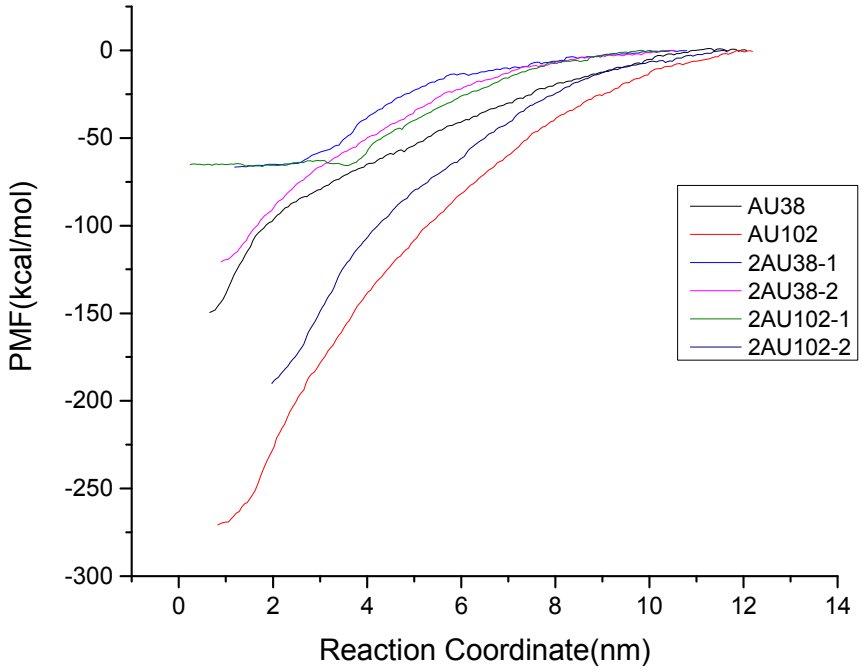

Fig. 8 Potential of mean force (PMF) profile for different model systems.